Lawrence Berkeley Laboratory

UNIVERSITY OF CALIFORNIA, BERKELEY, CA

Materials & Molecular Research Division

Submitted to Metallurgical Transactions

PRECIPITATION-STRENGTHENED AUSTENITIC Fe-Mn-Ti ALLOYS

K. M. Chang and J. W. Morris, Jr.

June 1979

Prepared for the U. S. Department of Energy
under Contract W-7405-ENG-48

DISCLAIMER

PRECIPITATION-STRENGTHENED AUSTENITIC Fe-Mn-Ti ALLOYS

K. M. Chang and J. W. Morris, Jr.

Department of Materials Science and Mineral Engineering and
Materials and Molecular Research Division, Lawrence Berkeley Laboratory;
University of California, Berkeley, California 94720

ABSTRACT

The precipitation of intermetallic compounds in the Fe-20Mn-2Ti and Fe-28Mn-2Ti alloy systems have been investigated over the temperature range 700°C to 900°C by hardness measurements, optical and scanning electron microscopy, and X-ray diffraction. In both systems only the equilibrium Laves phase was observed. The precipitate was identified as C14($MgZn_2$) type hexagonal Laves phase with a chemical composition close to Fe_2(Ti,Mn). In an as-annealed sample precipitation occurred in a heterogeneous manner, predominantly along grain boundaries. The effect of a cold deformation between the solution annealing and aging processes was also investigated. In addition to a high density of dislocations, martensitic phases were induced by deformation; a $\gamma \rightarrow \varepsilon$ transformation occurred in the Fe-28Mn-2Ti alloy while a $\gamma \rightarrow \alpha'$ transformation was predominant in the Fe-20Mn-2Ti alloy. Subsequent aging was conducted at temperatures above the A_f. A large number of very fine precipitates formed randomly in the matrix after a short aging period. This cold work plus aging treatment resulted in an increase in yield strength. The enhancement of mechanical properties is due to the randomly distributed precipitates combined with the high defect density and fine substructure.

INTRODUCTION

It is well known that manganese may sometimes be substituted for nickel in austenitic stainless steels, such as the AISI 200 series, to achieve an economic benefit without a significant sacrifice in relevant properties. The resulting high manganese austenite can be strengthened by mechanical work, as in the cold formed Fe-Mn-Cr alloys used for high strength retaining rings for electrical generators, or by the introduction of interstitial hardening elements, such as carbon or nitrogen, which contribute to the strength of the matrix by forming precipitates. However, processing difficulties and the thermal instability of deformation induced defect structures or interstitial precipitates place some limits on the usefulness of high manganese steels. For many applications it would be desirable to form high manganese steels which were strengthened by intermetallic precipitates. The identification of effective controllable intermetallic precipitates for strengthening high manganese steels awaits further research.

The occurrence of intermetallic phases in iron has been summarized by Nevitt[1]. Table I is a general resume of the known phases based on B elements such as manganese, iron, cobalt and nickel with additions of A elements from the titanium, vanadium, or chromium groups of the Periodic Table. Three factors, the electron/atom ratio, atomic size and compressibility, are important in determining alloy chemistry. The phases listed in Table I can be classified into two groups on the basis of the atomic arrangement within their crystal structures. In one group are the geometrically close packed phases which contain both octahedral and tetrahedral interstices, e.g. B_3A. In the other group are the topologically close packed phases which contain only tetrahedral interstices e.g. the Laves phases B_2A, sigma, mu, and chi. The B_3A structures are the most useful intermetallic compounds for strengthen-

ing austenitic iron alloys, due to their morphology, small interparticle spacing, coherency with the lattice, and the high ductility of these phases compared with those containing other precipitates.

Unfortunately, no phase of the B_3A type has been found in which the B element is manganese or iron. The most likely phase to occur in Fe-Mn austenite is the B_2A Laves phase which usually embrittles the alloy at room temperature but seems to have a strengthening effect at high temperatures.[2] The embrittlement caused by the Laves phases is due to a strong tendency to form continuous precipitates along grain boundaries. By eliminating this continuous grain boundary precipitation, Laves phases can be effectively utilized to strengthen an iron matrix. For example, Jin[3] successfully spheroidized the grain boundary Laves phase in ferritic Fe-Ta alloys by cycling through the α'-γ phase transformation, and achieved a substantial increase in alloy toughness.

The objective of the present study was to investigate precipitation behavior in Fe-Mn austenites containing titanium as the hardening element. Three aspects of the precipitation process were of particular interest: the precipitate type, the preferential precipitation sites, and the possibility of modifying the precipitate distribution by utilizing theremo-mechanical treatments. The precipitate type in the Fe-Mn-Ti ternary is currently unknown though the Laves phases Fe_2Ti and Mn_2Ti have been observed in the respective binary systems[4]. The existence of the compound Fe_2Mn in the Fe-Mn binary has been proposed by Soviet workers[5] though its existence is not commonly accepted. Given the known or tentative presence of phases of the Laves type in each of the relevant binary diagrams a Laves phase is anticipated in the Fe-Mn-Ti system. The Laves phases are, in general, heterogeneously nucleated, forming continuous precipitate films on the grain

boundaries. As a consequence, these precipitates do not contribute much alloy strengthening and are harmful to alloy ductility through their promotion of intergranular fracture.

The tendency toward intergranular precipitation of the Laves phase may, however, be partly avoided by introducing mechanical work prior to the aging process, to introduce a dense distribution of heterogeneous nucleation sites and also provide a defect structure to accelerate the diffusion of the precipitating intermetallic species. However, in Fe-Mn alloys of intermediate manganese content (approximately 14-28%Mn), the introduction of a dislocation structure through mechanical work is complicated by the phase instability of the austenite[6]. On deformation a high-manganese austenite may undergo mechanically induced transformations to either an ε martensite (HCP) or to the usual α' martensite (BCC). These transformations may complicate thermo-mechanical processing.

For purposes of this investigation two compositions were chosen: an Fe-20Mn-2Ti alloy, which is expected to be mechanically unstable with respect to the formation of both ε and α' martensites on low temperature deformation, and a richer austenite, Fe-28Mn-2Ti, which is anticipated to show increased stability with respect to transformation at room temperature and above.

I. EXPERIMENTAL PROCEDURE

The alloys used in this research were prepared by induction melting high purity (99.9%) iron, manganese, and titanium under argon atmosphere to produce cast ingots in 10 and 4.5 kg copper chill molds. The nominal and actual compositions of the alloys used in the present study are given in Table II. The ingots were homogenized at 1200°C for 24 hours under a partial pressure of argon gas (0.38 torr), forged to 26mm (for 10 kg ingots) and 13mm (for 4.5 kg ingots) thick plates, solution annealed at 1150°C for 1.5 hours under argon gas atmosphere, and water quenched. Some plates were cold rolled to about 40% reduction to study the effects of cold work on the precipitation reaction.

Tensile tests were conducted at room temperature in an Instron machine using flat tensile specimens of 25.4mm gauge length and 6.35mm x 3.175mm cross section at a cross-head speed of 2.0mm/min. Two specimens were tested for each data point. The 0.2% offset method was used to obtain the yield strength. The hardness of the specimens was measured as an average of five indentations.

Quantitative measurements of the amounts and types of phases present were made using an X-ray diffractrometer utilizing transverse sections of plates to minimize the effects of preferred orientation. The percentage of phases present was estimated by comparing the integrated diffraction intensities of the $(200)_\gamma$, $(10.1)_\varepsilon$, and $(200)_\alpha$, peaks from a copper K_α source . The structure of the precipitates was determined by X-ray diffraction. Their chemical compositions were studied using X-ray energy dispersion analysis (EDAX) on a scanning electron microscope.

Optical metallographic specimens were chemically polished and etched using a 5% nital solution. Schumann's reagent (100ml cold saturated Na_2SO_3+5gm.

K_2SO_4) was applied whenever the ε martensite phase existed in a specimen since this reagent is reported[7] to be useful for delineating the ε phase. Thin foils for transmission electron microscopy were prepared by a jet electropolishing technique using a conventional chromic-acetic electrolyte. A Hitachi HU-125 electron microscope operated at 100 kV was used for the transmission microscopy.

II. RESULTS AND DISCUSSIONS

A. PHASE RELATIONS

The volume fractions of the phases present after various thermal or thermo-mechanical treatments as determined by X-ray diffraction are listed in Table III. Fe-Mn alloys having more than 28 wt%Mn are fully austenitic(γ) at room temperature. The hexagonal ε phase was not detected by X-ray diffraction in an as-annealed Fe-28Mn alloy, but traces of ε phase were observed under the optical microscope (Fig. 1a). In the alloy with 20 wt%Mn, ε phase (up to 70%) formed upon cooling to room temperature after solution annealing. A typical microstructure of mixed γ and ε phases is shown in Fig. 1b. No body-centered cubic α' phase formed in either of the binary Fe-Mn alloys even on cooling to liquid nitrogen temperature (-196°C). These results are consistent with previous observations.[6]

With the addition of titanium the amount of ε decreases dramatically and more γ phase is retained at room temperature. The Fe-28Mn-2Ti alloy was completely austenitic in the as-annealed condition (Fig. 1c). Less than 10% of ε phase formed in the Fe-20Mn-2Ti alloy (Fig. 1d). The influence of Ti on the $\gamma \rightarrow \varepsilon$ transformation is not well understood. Previous research[8] suggests that titanium additions can reduce the stacking fault energy of som austenitic Fe-Ni-Cr alloys, which should promote the formation of ε phase; however, the effect of Ti on the stacking fault energy of Fe-Mn austenites is

unknown. It is clear from the present results that Ti stabilizes Fe-Mn austenite with respect to ε formation. This was further shown by aging Fe-20Mn-2Ti alloys for long period to precipitate Ti out of the matrix. Isothermal overaging at 800°C for 20 days left about 1% of the titanium in the matrix; the volume fraction of the ε phase increased again to 44% (Table III).

B. KINETICS AND MORPHOLOGY OF LAVES PHASE PRECIPITATION

1. Precipitation in the Fe-20Mn-2Ti alloy:

The influence of temperature on age hardening kinetics is shown in Fig. 2. As expected, the lower the aging temperature, the longer the time required to reach maximum hardness. The hardening response of the alloy was very slow in the temperature range 700°C to 900°C; more than 100 hours aging was required to achieve maximum hardness. No secondary hardening was observed, suggesting that a single precipitation process occurred.

On aging, precipitates nucleated first at grain boundaries and grew continously until a heavy network was formed (Fig. 3a). Just prior to the significant hardness increase precipitates began to form within the grains. As the aging time increased, intragranular precipitation became more pronounced and the hardness increased. The intragranular precipitates formed preferentially along planes parallel to γ - ε phase boundary. After extensive aging the continuous grain boundary precipitates began to break up and spheroidize (Fig. 3b).

The alignmemt of precipitates along the prior γ - ε interfaces requires some comment. Though the γ - ε interfaces do not exist when the alloy is heated up to the aging temperature, which is above A_f (∿540°C), the distortion energy due to the martensitic transformation may still remain[9] to help the nucleation process. A high density of stacking faults inside grains

introduced by the $\varepsilon \rightarrow \gamma$ transformation of the Fe-20Mn-2Ti alloy might also serve as the nucleation site for precipitation.

2. Precipitation in the Fe-28Mn-2Ti Alloy:

The hardening kinetics of the Fe-28Mn-2Ti alloy are shown as a function of aging temperature in Fig. 4. The age hardening response is similar to that observed in the Fe-20Mn-2Ti alloy, suggesting that the same precipitation reaction takes place. The aging response is more temperature dependent in this completely austenitic alloy. The hardness approaches its plateau within 100 hours at 900°C but there was no obvious hardness increase in a sample aged at 700°C for more than 200 hours. Though the as-annealed hardness varied between the two alloys (R_B 72 for Fe-20Mn-2Ti and R_B 62 for Fe-28Mn-2Ti), the total hardness increase to the plateau is almost the same. The hardness result can be interpreted by reference to the morphology and distribution of precipitates. Fig. 5 shows a series of micrographs from samples aged at 800°C. In the early stages continuous precipitation developed rapidly along grain boundaries but contributed no hardness increase. The continuous precipitates can also be found along the incoherent interfaces of annealing twins but few precipitates occurred on coherent interfaces. The precipitation occurs in a heterogeneous manner on high energy surfaces. Random nucleation started within grains when most of the high energy surface had been utilized. The hardness gradually increased as the percentage of precipitates observed in grains increased. Spheroidization of grain boundary precipitates was also observed during the final stage of aging.

C. PRECIPITATE IDENTIFICATION

Samples of both alloys were aged at 800°C for 20 days to obtain precipitate sizes and volume fractions adequate for analysis. It is necessary to obtain precipitates with diameters greater than 2μm for EDAX analysis and more than 5% in volume for X-ray diffraction.

A number of extra diffraction peaks were present in the X-ray diffraction

patterns. The corresponding interplanar spacings and relative intensities are listed in Table IV. These closely match the values in the ASTM Powder Diffraction File for Fe_2Ti.[10] The crystal structure of the precipitate is the hexagonal Laves phase ($MgZn_2$ type, C14); each unit cell consists of 12 atoms as sketched in Fig. 6. The "a" parameter of the precipitate was determined from the (h k 0) reflections, using the extrapolation function of Nelson and Riley.[11] The "c" parameter was determined from the (00ℓ) reflection by the method of Taylor and Floyd[12] for hexagonal crystals. The values obtained are a = 4.780Å, c = 7.788Å, and c/a = 1.629 .

To obtain information about the chemical composition of the precipitates an SEM-EDAX study was made. Overaged specimens were examined in the scanning electron microscope, and some large precipitates (∿5μm diameter) were chosen for EDAX analysis. Fig. 7 presents comparative energy spectra showing that the precipitates are rich in titanium and that they also contain manganese. The computer-analyzed data are given in Table V. The results are almost identical for the two alloys. The fraction of Fe in the precipitates is about 2/3, while that of the sum of Mn and Ti is about 1/3. Extraction replicas of specimens were also made. The results confirmed the above observations. The identity of the precipitates thus appears to be $Fe_2(Ti,Mn)$ in both alloys. The crystal structure of the precipitates is like that of Fe_2Ti, with Mn atoms apparently substituting at Ti lattice sites. It is possible that a small fraction of Mn atoms replace Fe atoms in the precipitates explaining why the measured Fe concentration is somewhat less than the ideal stoichiometric ratio, 2/3.

D. EFFECTS OF COLD WORK ON PRECIPITATION

It is not surprising that direct precipitation of Laves phases does not strengthen the solution-treated Fe-Mn-Ti austenites significantly. The interparticle spacing between the aged precipitates formed inside grains is too large to be an effective obstacle to dislocation motion. A cause

of this ineffective precipitation is the absence of beneficial nucleation sites within the grains for precipitation of Laves phase. In an attempt to overcome this problem the alloys were cold deformed ($\sim$ 40% reduction) between the solution annealing and the aging treatments.

The mechanical instability of high Mn austenites has been investigated by many previous workers.[6,13,14] These alloys undergo a partial martensitic phase transformation under heavy deformation at room temperature. In addition to the increase of defect and dislocation density, cold work induces elastic and plastic strain energy which raises the transformation temperature to above ambient temperature. The volume fraction of induced phases in the cold-worked samples is shown in Table III. In the Fe-20Mn-2Ti alloy, a large amount of α' martensite and some ε phase appeared after cold rolling. Electron microscopy revealed that the induced α' phase is dislocated martensite with a high density of dislocations inside the martensite lathes (Fig. 8). Thin sheets of induced ε phase formed in the Fe-28Mn-2Ti alloy during cold working, but no α' phase was observed. The induced ε sheets are wavy and bent though they are parallel to one another in series. More detailed examination by electron microscopy (Fig. 9) reveals a high dislocation density in the untransformed matrix.

Like the usual martensite obtained by thermal treatment, the induced phase, ε or α', in the cold worked alloys reverts to austenite when the sample is reheated to high temperature. The dilatometry results indicated that the A_f is approximately 540^{o}C.

The Fe-20Mn-2Ti alloy was reheated to 800°C after cold-rolling, and then aged at that temperature. The precipitation kinetics are accelerated by predeformation. Very fine precipitates of Laves phase decorated the entire structure after one hour aging (Fig. 10a). The precipitates were randomly distributed; no continuous grain boundary precipitate was found. The very low diffusivity of the substitutional elements, Mn or Ti, in the austenite

matrix makes precipitate growth or coarsening very difficult. No evidence of overaging was observed even after aging for 96 hours (Fig. 10b). After the cold work had been fully recovered the alloy maintained a high level of hardness ($R_C \sim 26$).

Closer examination of the precipitates formed in the cold worked plus aged alloys was carried out in the electron microscope. It was not possible to determine the orientation relations of the precipitates with respect to the matrix due to the heavy deformation of the latter. In the Fe-28Mn-2Ti alloy, the precipitates were aligned in a specific orientation, which was believed to lie in the stacking fault plane. The precipitate size was less than .3μm. A high density of dislocations still remained in the matrix after aging for one hour at 700°C (Fig. 11a). The precipitates formed in the Fe-20MN-2Ti alloy were denser and more random in distribution. Lath boundaries of previous α' martensites were decorated by precipitates in some instances, but no continuous networks were observed (Fig. 11b).

E. MECHANICAL PROPERTIES

Both as-annealed alloys exhibited a low yield strength (∿30ksi) and high elongation (∿75%). X-ray diffraction of the broken tensile specimens showed phase contents similar to those obtained after cold rolling; the mechanically induced transformation also occurs during tensile testing. In both stress-strain curves the ultimate tensile strength, at which the tensile specimen began to neck, was delayed to a large elongation with a very low strain hardening rate. The final fracture of the specimen occurred rapidly after passing the ultimate point. This is a typical feature of alloys with a mechanically induced transformation. The ultimate tensile strength increases as the extent of deformation-induced transformation increases. The higher tensile strength of the Fe-20Mn-2Ti alloy is apparently due to the introduction of α' martensite.

Specimens aged after annealing reached full hardness after 100 hours at 800°C. The resulting grain size is large, (200∿500μm), and the grains are coated by a nearly continous network of Laves phase. As anticipated, broken tensile specimens of both alloys exhibit an intergranular fracture mode (Fig. 12). No significant strengthening accompanied precipitation. The yield strength increased by ∿5 ksi for the Fe-28Mn-2Ti alloy and 10 ksi for the Fe-20Mn-2Ti alloy.

The stress-strain curves of the alloys which were cold worked and/or aged at 700°C for one hour are shown in Fig. 13. The yield strength was observed to increase to 107 ksi for the Fe-20Mn-2Ti alloy and to 90 ksi for the Fe-28Mn-2Ti alloy by use of the cold-working plus aging treatment. Unlike the cold worked alloys, which reached ultimate strength without much plastic deformation, the cold work plus aging alloys exhibited retarded necking with very large uniform elongation. This is believed to be the result of mechanically induced transformation.

The yield strength, tensile strength, and elongation of alloys after the cold work plus aging treatment are shown as a function of aging temperature in Fig. 14. Given a one hour aging, both alloys showed a monotonically decreasing yield strength for increasing aging temperature. The elongation showed a peak in the temperature range 650°C to 800°C. No obvious change in elongation was observed for aging times up to 4 hours, although the yield strength kept decreasing with aging time as the deformation-induced defect structure recovered. The fracture surfaces of the broken tensile specimens were unusual, in that they neither showed the dimpled rupture mode typical of the as-annealed or the cold worked samples nor the brittle intergranular cleavage showed by the aged specimens. For the Fe-20Mn-2Ti alloy, in which the $\gamma \rightarrow \alpha'$ transformation is predominant on deformation, a fracture surface perpendicular to the tensile axis was formed. Tiny cups

and cones populated the fracture surface (Fig. 15a). On the other hand, the Fe-28Mn-2Ti alloy, in which only the $\gamma \rightarrow \varepsilon$ transformation occurred, exhibited a fracture surface consisting of several tilted planes. In addition to dimple rupture, a lamellar pattern was observed (Fig. 15b). The exact mechanism responsible for these fracture surfaces has not been established.

III. CONCLUSIONS

1. Precipitation in the Fe-20Mn-2Ti and Fe-28Mn-2Ti systems proceeds by the formation of single particles of equilibrium Laves phase, $Fe_2(Mn,Ti)$, hexagonal C14 type ($MgZn_2$). No transition phase was detected.
2. Precipitation in the as-annealed structure occurs by heterogeneous nucleation; heavy networks of Laves phases form first along the grain boundary before individual precipitates appear inside grains. No significant age-hardening is observed but intergranular fracture takes place due to the Laves phase precipitates.
3. Cold rolling after solution annealing provides numerous efficient nucleation sites beneficial to subsequent aging. The precipitate nucleation site changes from the grain boundary to separate heterogeneous sites inside grains. A desirable microstructure, in which fine precipitates are randomly distributed, is then obtained.
4. Enhancement of the mechanical properties of Fe-Mn austenites can be achieved through the combination of cold work, precipitation, and mechanically induced transformation.
5. Titanium additions stablize the austenite in Fe-Mn alloys.

ACKNOWLEDGMENTS

This work was supported by the Division of Materials Sciences, Office of Basic Energy Sciences, U. S. Department of Energy under Contract No. W-7405-Eng-48.

The authors wish to thank Professor V. F. Zackay and Professor I. Finnie for helpful discussions.

REFERENCES

1. M.V. Nevitt: Electronic Structure and Alloy Chemistry of the Transition Elements, P. 101, Interscience Publishers, New York, 1963.
2. K. Bungardt and G. Lennartz: Arch. Eisenh., 1962, Vol, 33, p. 251.
3. S. Jin: M.S. Thesis, U. of Calif., Berkeley, California, (1971).
4. M. Hansen: Constitution of Binary Alloys, McGraw-Hill, New York, 1958.
5. E.M. Sokolovskaya, A.T. Grigorév, and Y.F. Altunin: Russ. J. Inorg. Chem., 1962, Vol. 7, p. 1464.
6. C.H. White and R.W.K. Honeycombe: J. Iron Steel Inst., 1962, Vol, 200, p. 457.
7. H. Schumann: Arch. Eisenh., 1967, Vol. 38, p. 647.
8. S. Barnartt, R. Stickler, and D. van Rooyen: Corrosion Sci., 1963, Vol. 3, p. 9.
9. G. Krauss, Jr. and M. Cohen: Trans, TMS-AIME, 1962, Vol. 224, p. 1212.
10. G.R. Speich: Trans. TMS-AIME, 1962, Vol. 224, p. 850.
11. J.B. Nelson and D.P. Riley: Proc. Phys. Soc. (London), 1945, Vol. 57, p. 60.
12. A. Taylor and R.W. Floyd: Acta Cryst., 1950, Vol. 3, p. 285.
13. D.J. Drobjak and J. Gordon Parr: Met. Trans., 1970, Vol. 1, p. 1521.
14. K. Sipos, L. Remy, and A. Pineau: Met. Trans. A, 1976, Vol. 7A, p. 857.

Table I. OCCURRENCE OF PHASES IN BINARY AND TERNARY TRANSITION ELEMENT SYSTEMS

B Transition Element	A Element: Group IV (4e/a)			Group V (5e/a)			Group VI (6e/a)			BB'
	Ti	Zr	Hf	V	Nb	Ta	Cr	Mo	W	
Mn (7e/a)	B_2A	B_2A	B_2A		B_2A	B_2A				
				BA						
	χ	χ	χ	χ	χ	χ	χ	χ	χ	
	σ			σ			σ	σ		
Fe (8e/a)	B_2A	B_2A	B_2A		B_2A	B_2A		B_2A	B_2A	
				BA						FeAl
	χ			χ				χ		FeCo
				σ	σ	σ	σ	σ		
Co (9e/a)	B_2A	B_2A	B_2A	B_3A	B_2A	B_2A		B_3A	B_3A	
	BA	BA	BA							CoAl
				χ				μ	μ	
	G	G	G	σ	G	G	σ	σ		
Ni (10e/a)	B_3A			B_3A	B_3A			B_3A		
	BA			χ						β
				σ	μ	μ	σ			(NiAl)
	G	G	G	G	G	G				

* μ: B_7A_6; G: $A_6B_{16}Si_7$; σ: $B_4A \sim BA_4$; χ: $B_4A \sim BA$

Table II. CHEMICAL COMPOSITION OF ALLOYS

Ingot No.	Weight	Designation	Composition wt%		
			Fe	Mn	Ti
755-1	10 kg	Fe-20Mn	Bal.	19.11	--
755-2	10 kg	Fe-20Mn-2Ti	Bal.	18.66	1.70
7511-4	4.5 kg	Fe-28Mn-2Ti	Bal.	27.29	1.59
7511-10	4.5 kg	Fe-28Mn	Bal.	27.34	--
766-17	10 kg	Fe-20Mn-2Ti	Bal.	19.07	1.74
766-18	10 kg	Fe-28Mn-2Ti	Bal.	27.93	1.69

The impurity levels: C = 0.004%; N = 0.002%; O = 0.002%; P = 0.004%; Si < 0.01%; S = 0.006%.

Table III. DETERMINATION OF VOLUME PERCENTAGE OF PHASE PRESENT BY X-RAY ANALYSIS

Designation	Treatment	Phase volume percentage		
		γ	ε	α'
Fe-20Mn	AN	30.0	70.0	--
Fe-20Mn-2Ti	AN	90.4	9.6	--
Fe-20Mn-2Ti	AN+800°C/20 days	56.0	44.0	--
Fe-20MN-2TI	AN+CW	51.0	20.0	29.0
Fe-20Mn-2Ti	AN+CW+800°C/96 hrs	91.2	8.8	--
Fe-28Mn	AN	100.0	--	--
Fe-28Mn-2Ti	AN	100.0	--	--
Fe-28Mn-2Ti	AN+800°C/20 days	100.0	--	--
Fe-28Mn-2Ti	AN+CW	93.6	6.4	--
Fe-28Mn-2Ti	AN+CW+700°C/1 hr	100.0	--	--

AN: Annealed at 1150°C for 1.5 hrs.

CW: 40% reduction of cold rolling.

Table IV. INTERPLANAR SPACING OF THE PRECIPITATES

Precipitates				Standard values for Fe_2Ti	
2θ*	d	I/I_1	(hkℓ)	d	I/I_1
--	--	--	100	4.133	10
--	--	--	002	3.889	10
--	--	--	101	3.649	10
37.6	2.390	30	110	2.388	30
41.0	2.199	90	103	2.199	100
--	--	--	200	2.068	10
44.4	2.039	90	112	2.038	100
45.3	2.001	100	201	1.998	100
46.6	1.947	40	004	1.947	30
49.85	1.828	20	202	1.828	30
51.8	1.763	10	104	1.760	10
--	--	--	203	1.620	10
--	--	--	300	1.382	10
70.2	1.339	40	123	1.341	60
72.65	1.330	40	006	1.302	60
76.4	1.246	30	205	1.247	60
--	--	--	124	1.223	10
80.25	1.195	40	220	1.196	60

*CuKα radiation with λ = 1.54Å

Table V. DETERMINATION OF CHEMICAL COMPOSITION OF THE PRECIPITATES BY EDAX

Designation		Concentration (wt%)		
		Fe	Mn	Ti
Fe-20Mn-2Ti	matrix	78.90	19.44	1.66
	precipitate	63.60	14.80	21.60
Fe-28Mn-2Ti	matrix	69.76	29.34	0.90
	precipitate	62.90	14.30	22.80

*Specimens were aged at 800°C for 20 days.

FIGURE CAPTIONS

1. Optical micrographs of as-annealed Fe-Mn(-Ti) alloys: (a) Fe-28Mn; (b) Fe-20Mn; (c) Fe-28Mn-2Ti; (d) Fe-20Mn-2Ti.
2. Age-hardening curves of the Fe-20Mn-2Ti alloy.
3. Precipitation of the Fe-20Mn-2Ti alloy aged at 800°C for: (a) 2 hrs; (b) 48 hrs.
4. Age-hardening curves of the Fe-28Mn-2Ti alloy.
5. Precipitation of the Fe-28Mn-2Ti alloy aged at 800°C for: (a) 4 hrs; (b) 16 hrs; (c) 48 hrs.
6. Atomic arrangement in the unit cell of the C14($MgZn_2$) crystal.
7. EDAX for the precipitation of the Fe-20Mn-2Ti alloy.
8. Transmission electron micrograph of the cold-rolled Fe-20Mn-2Ti alloy.
9. Transmission electron micrograph of the cold-rolled Fe-28Mn-2Ti alloy: (a) bright field; (b) dark field.
10. Microstructures of the worked plus aged Fe-20Mn-2Ti alloy: (a) CW+700°C 1hr; (b) CW+700°C 96hrs.
11. Transmission electron micrographs of worked plus aged specimens: (a) Fe-28Mn-2Ti; (b) Fe-20Mn-2Ti.
12. Tensile fracture surfaces of simple aged specimens: (a) Fe-20Mn-2Ti; (b) Fe-28Mn-2Ti.
13. Engineering strain-stress curves of cold-worked and worked plus aged specimens.
14. The effect of aging temperature (for 1hr) on strength and elongation of cold-worked specimens.
15. Tensile fracture surfaces of worked plus aged specimens; (a) Fe-20Mn-2Ti; (b) Fe-28Mn-2Ti.

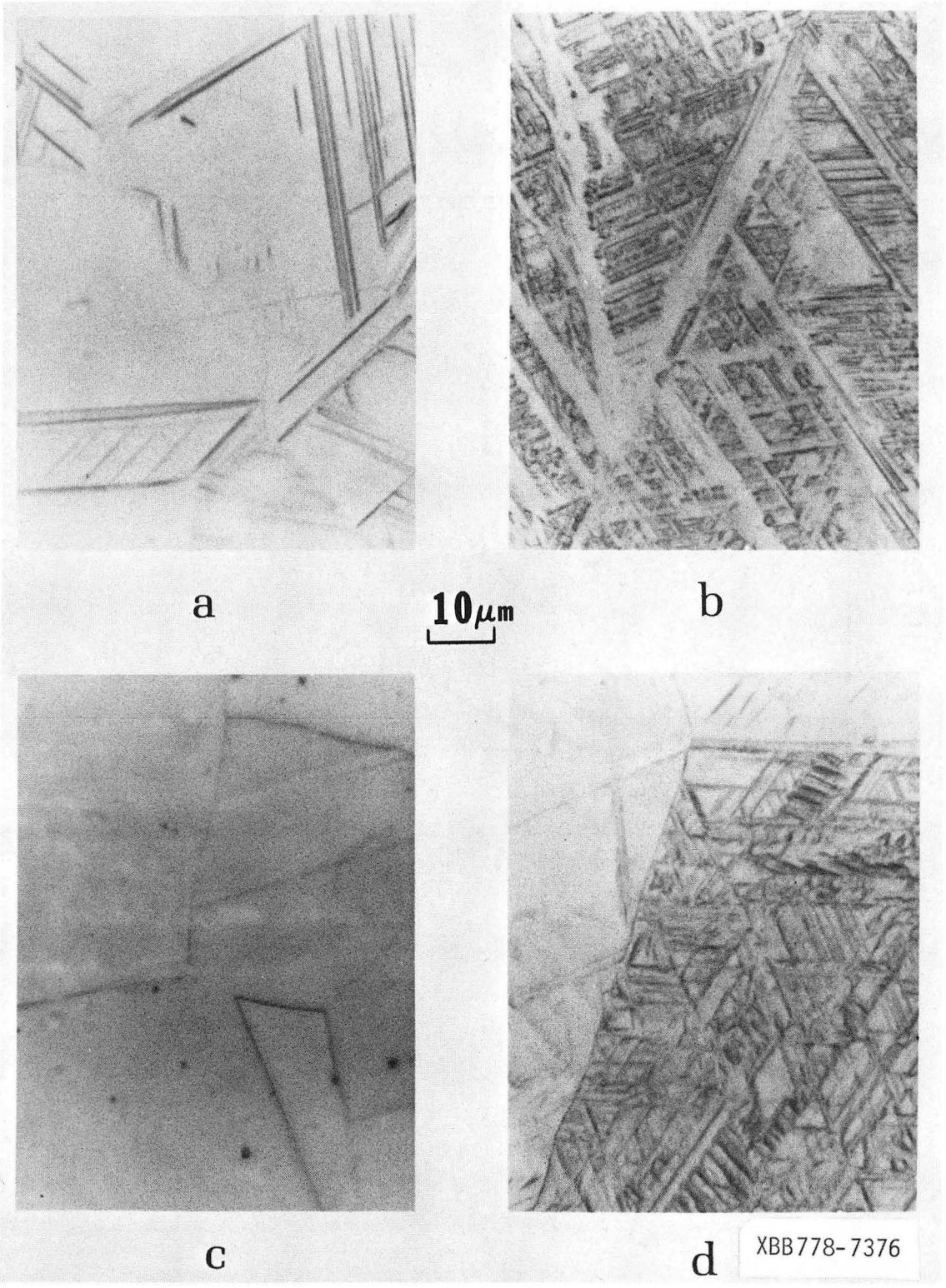

Fig. 1

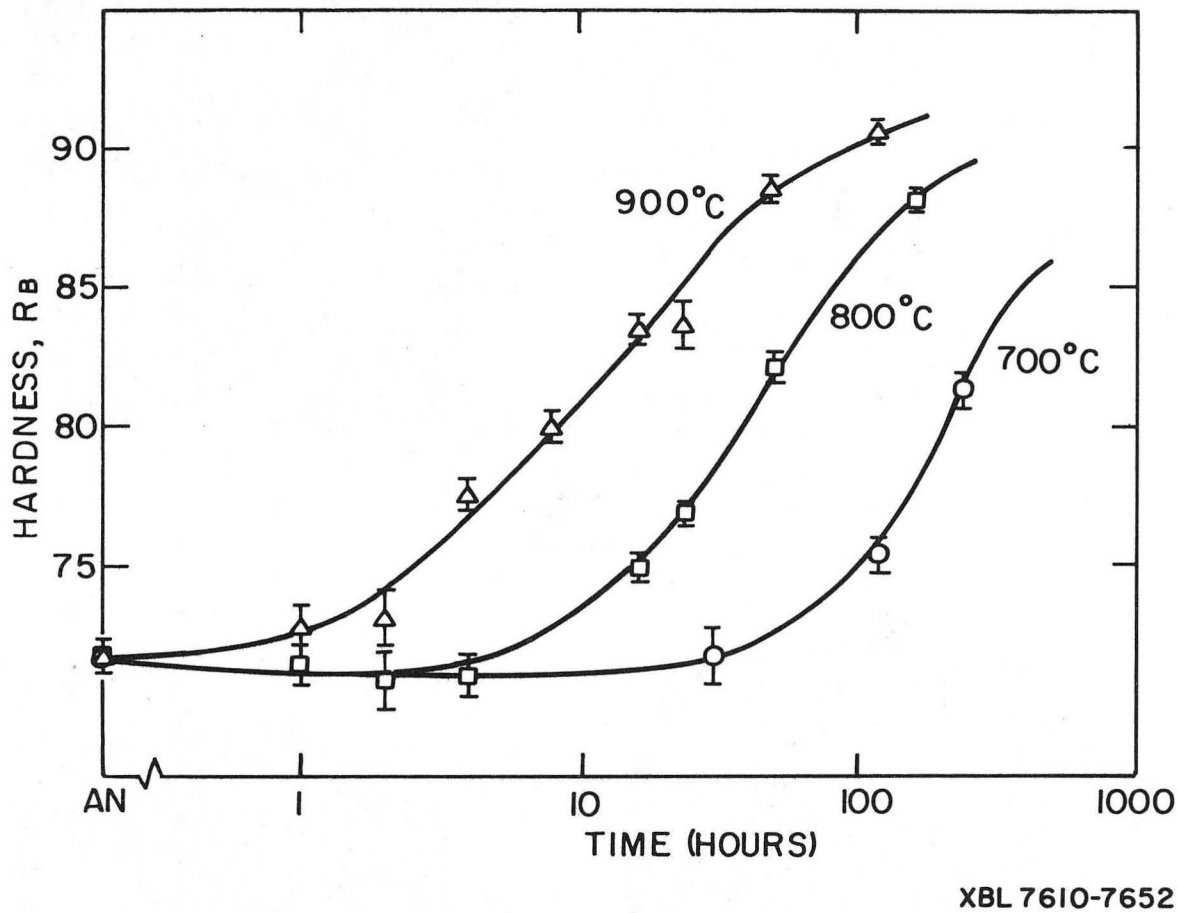
90
85
80
75
HARDNESS, RB
900°C
800°C
700°C
AN
1
10
100
1000
TIME (HOURS)
XBL 7610-7652

Fig. 2

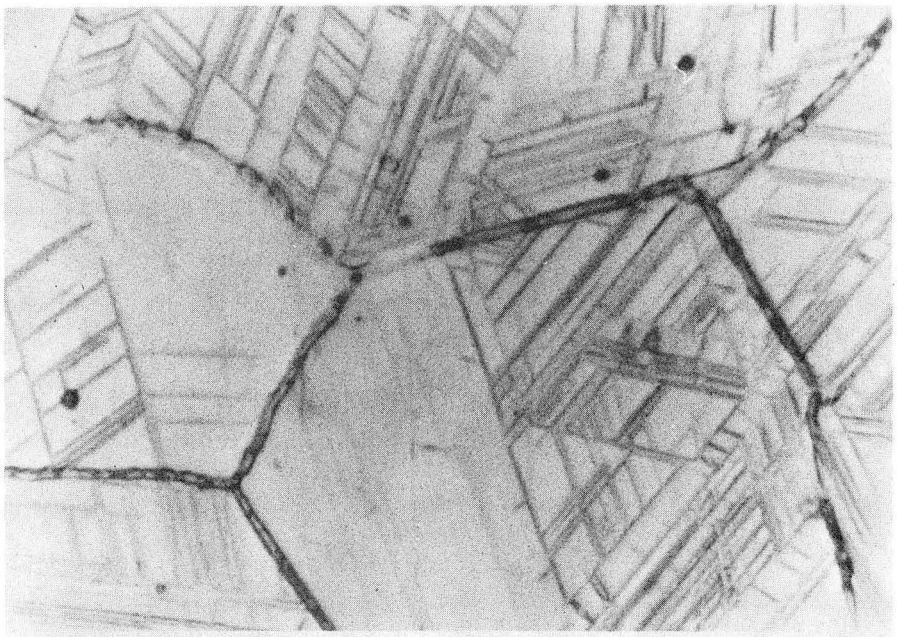

a

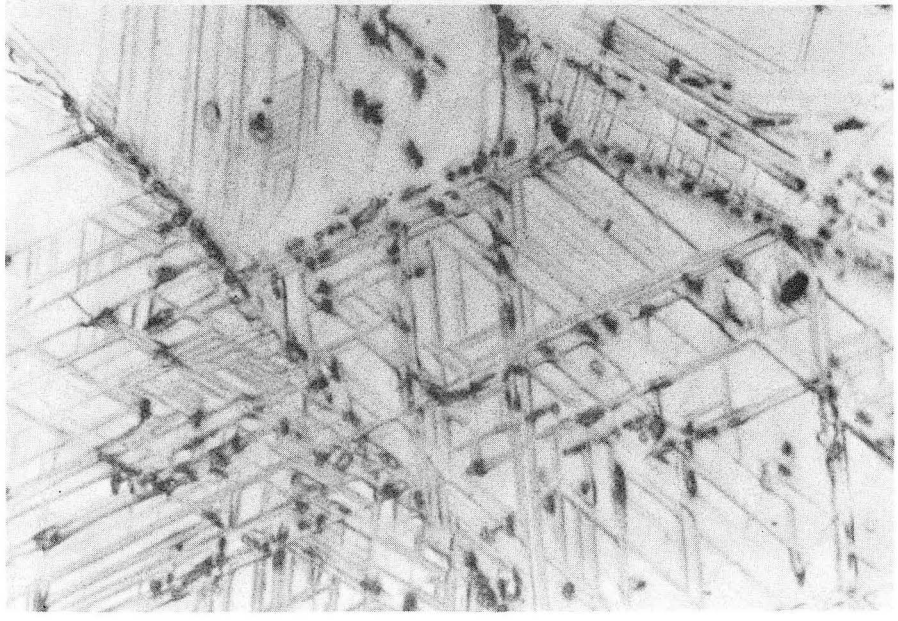

b

XBB769-8584

Fig. 3

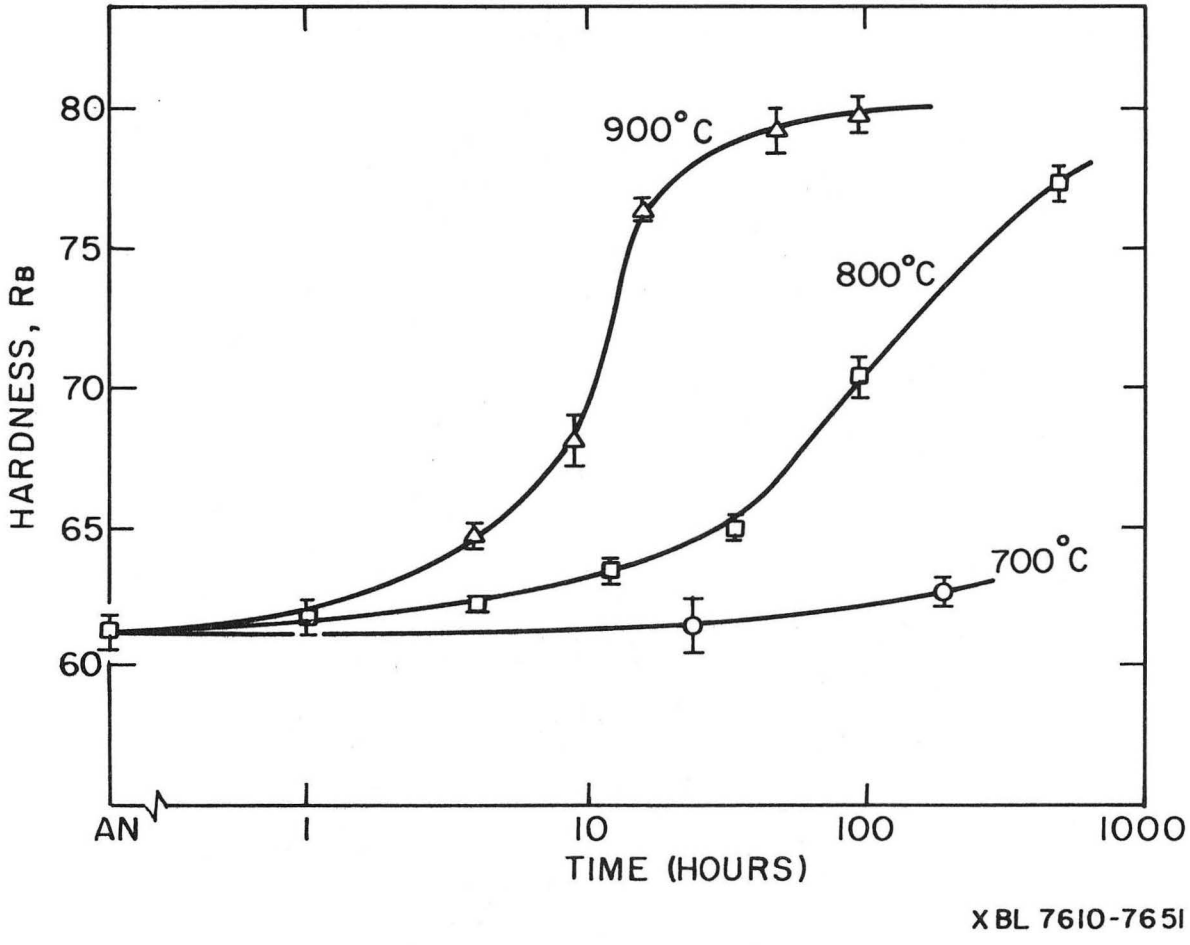
80
75
70
65
60
HARDNESS, RB
900°C
800°C
700°C
AN
1
10
100
1000
TIME (HOURS)
XBL 7610-7651

Fig. 4

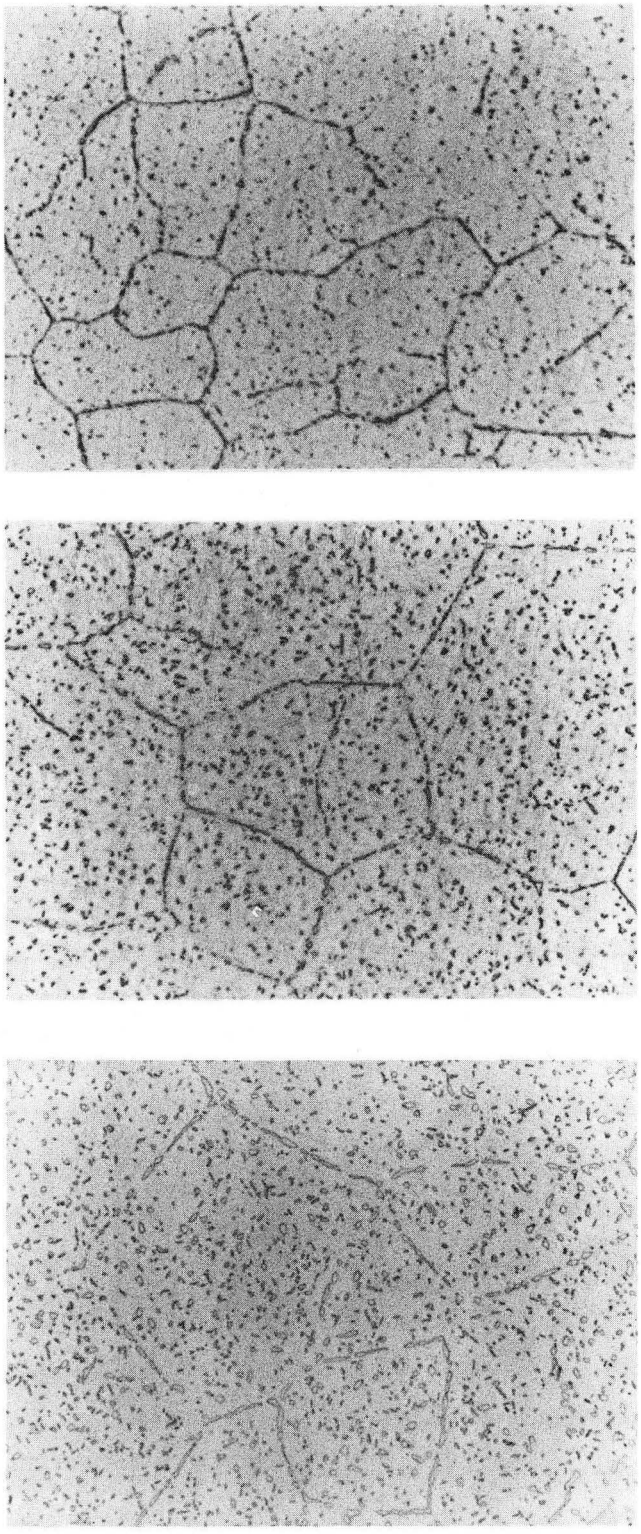

XBB760-10431

Fig. 5

C 14 ($MgZn_2$ type) Hexagonal D_{6h}^4 - P $6_3/mmc$

4Mg (C_{3v}): $\pm(\frac{1}{3}, \frac{2}{3}, z), \pm(\frac{1}{3}, \frac{2}{3}, \frac{1}{2}-z)$; $z = \frac{1}{16}$

2Zn (D_{3d}): $(000), (00\frac{1}{2})$

6Zn (C_{2v}): $\pm(X, 2X, \frac{1}{4}), \pm(\bar{2}X, \bar{X}, \frac{1}{4})$; $X = \frac{1}{6}$

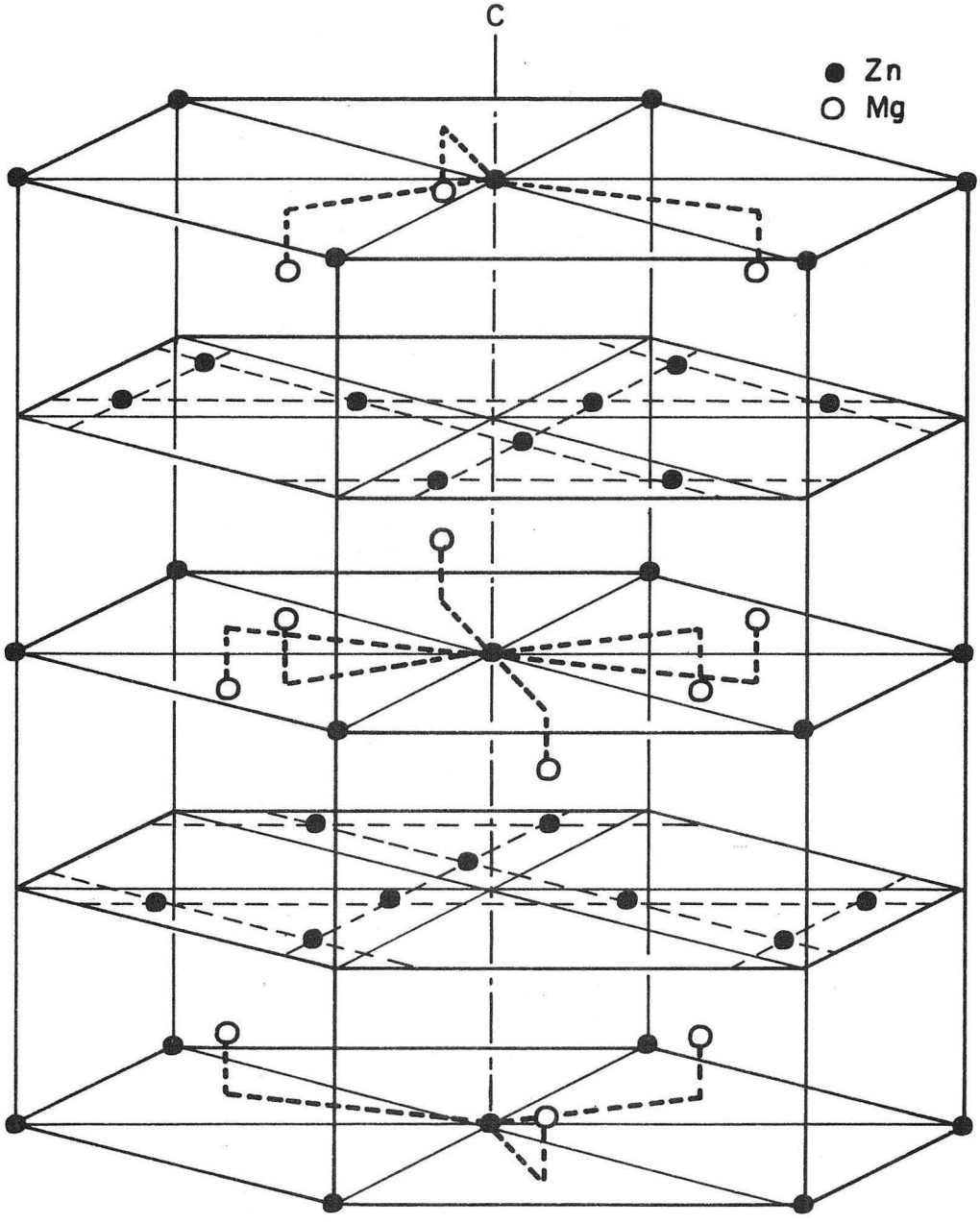

XBL7611-7810

Fig. 6

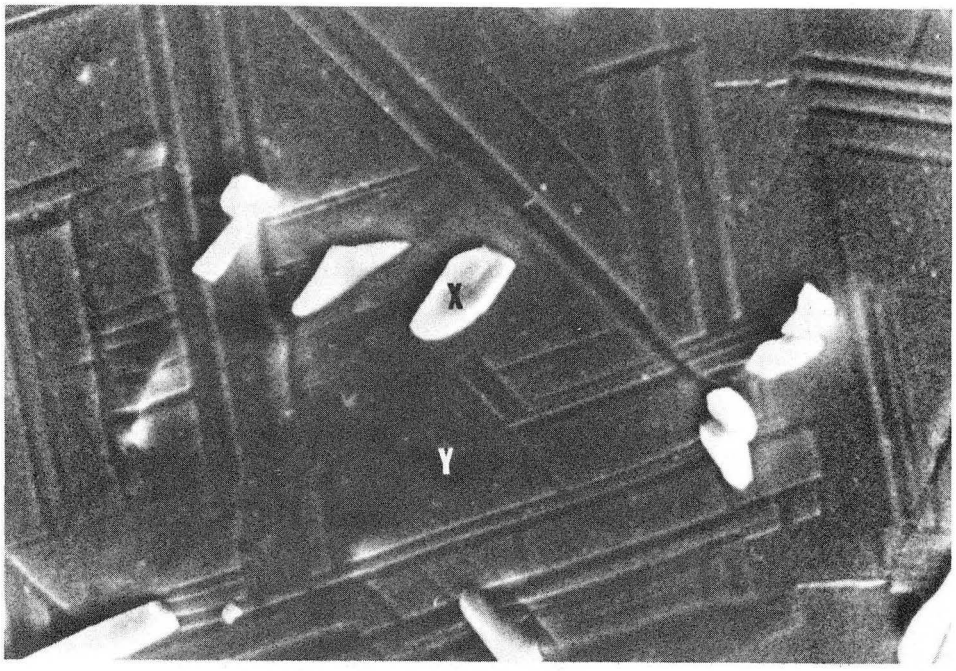

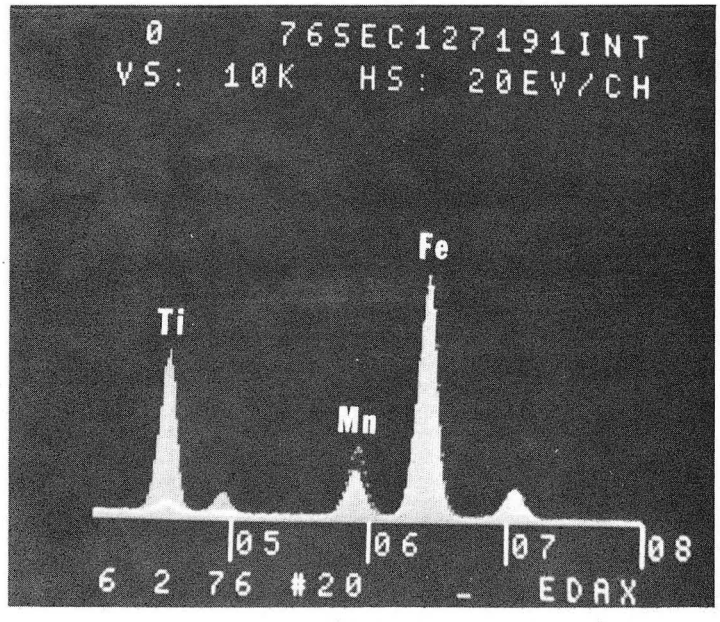

XBB769-8583

Fig. 7

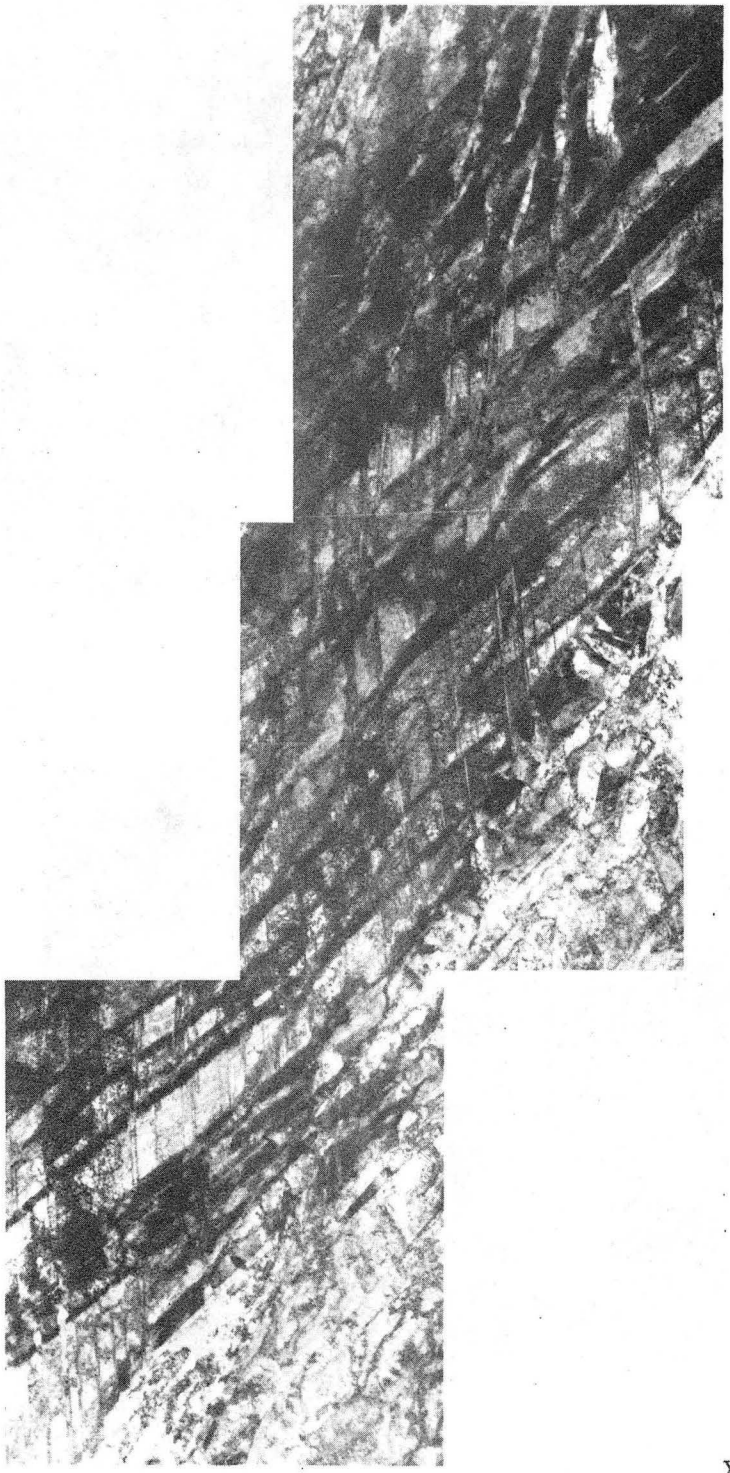

XBB773-1950

Fig. 8

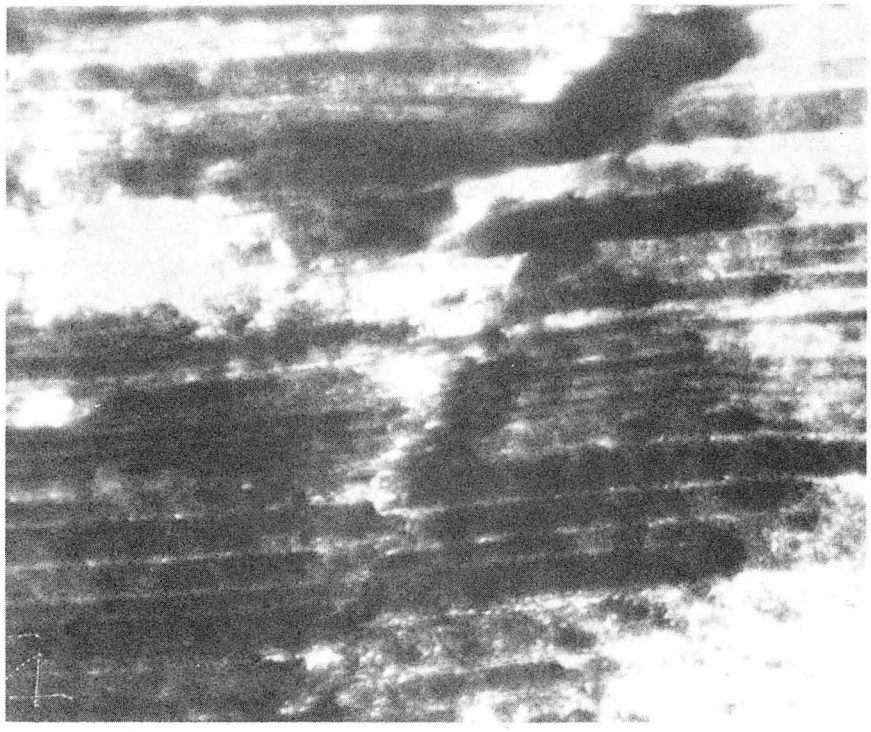

DF

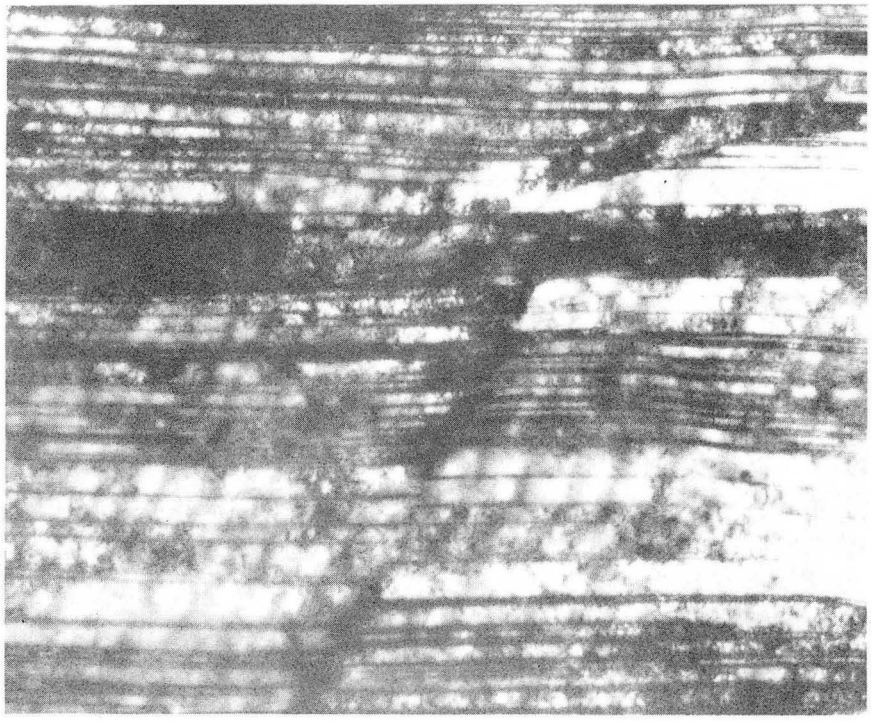

BF

XBB773-1948

Fig. 9

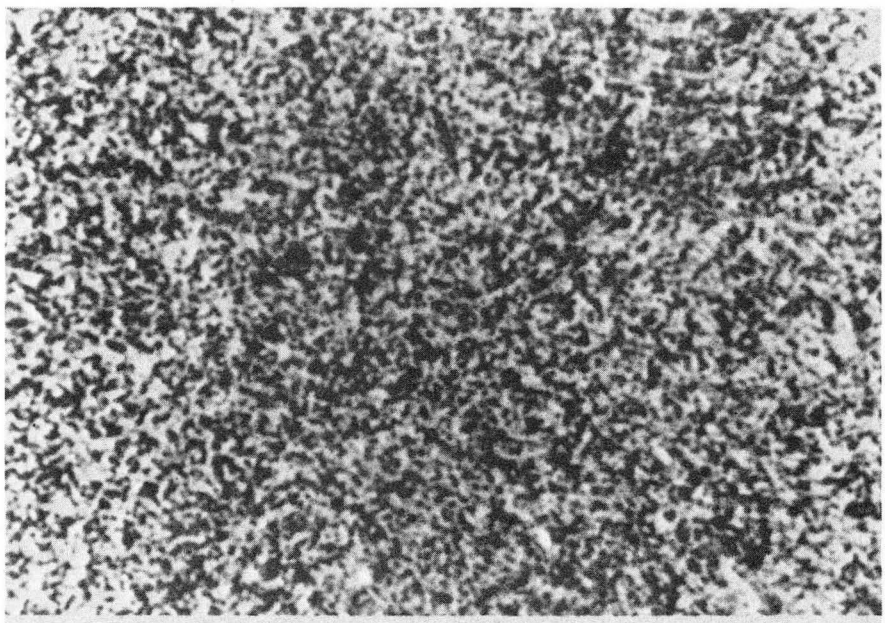

a

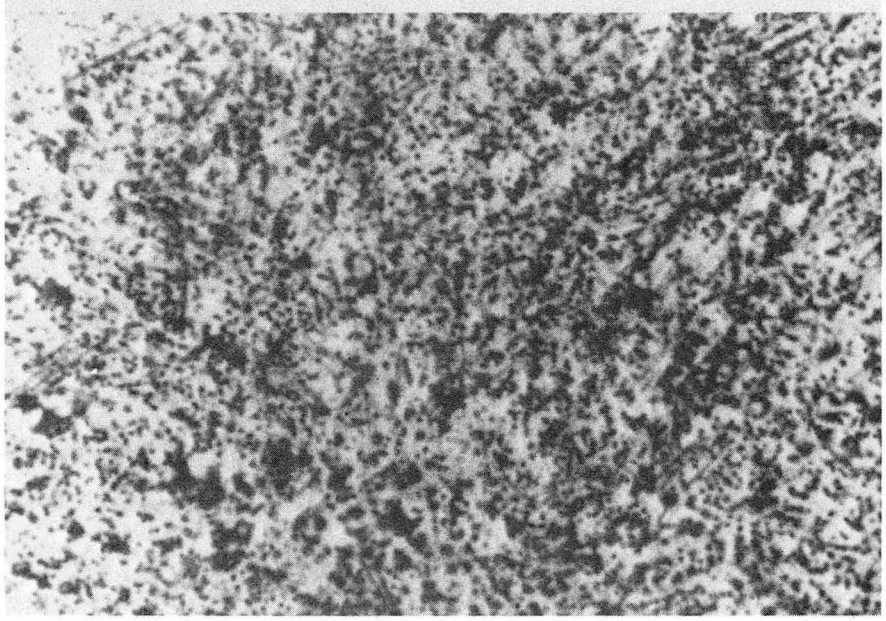

b

XBB769-8586

Fig. 10

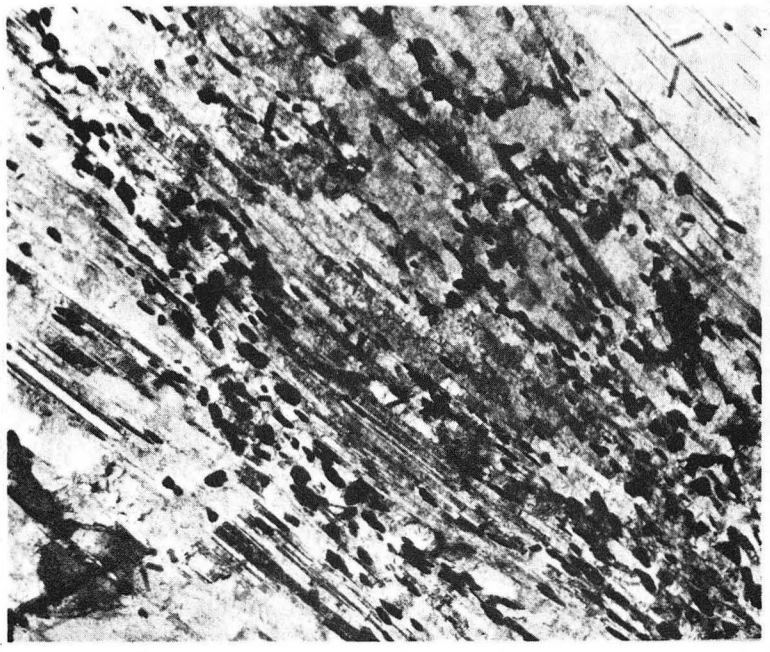

a

1 μm

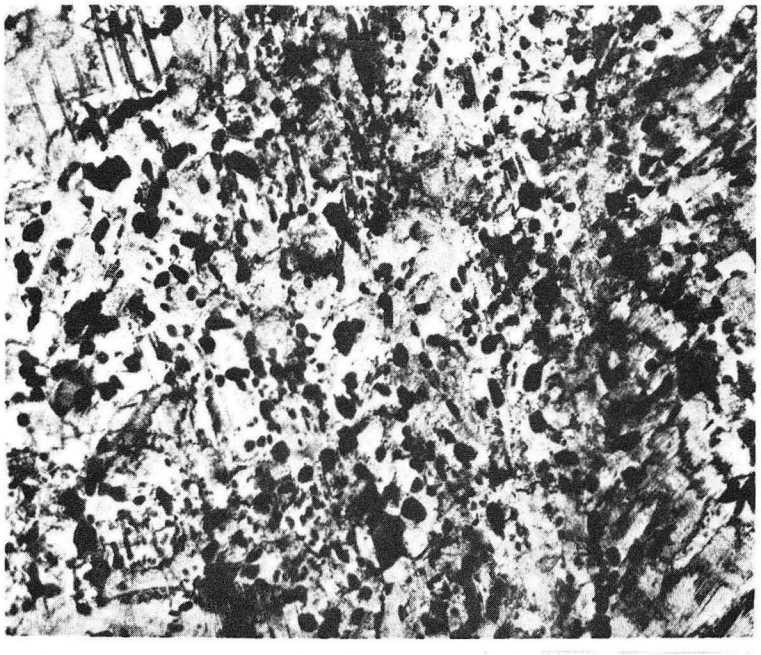

b

XBB777-7378

Fig. 11

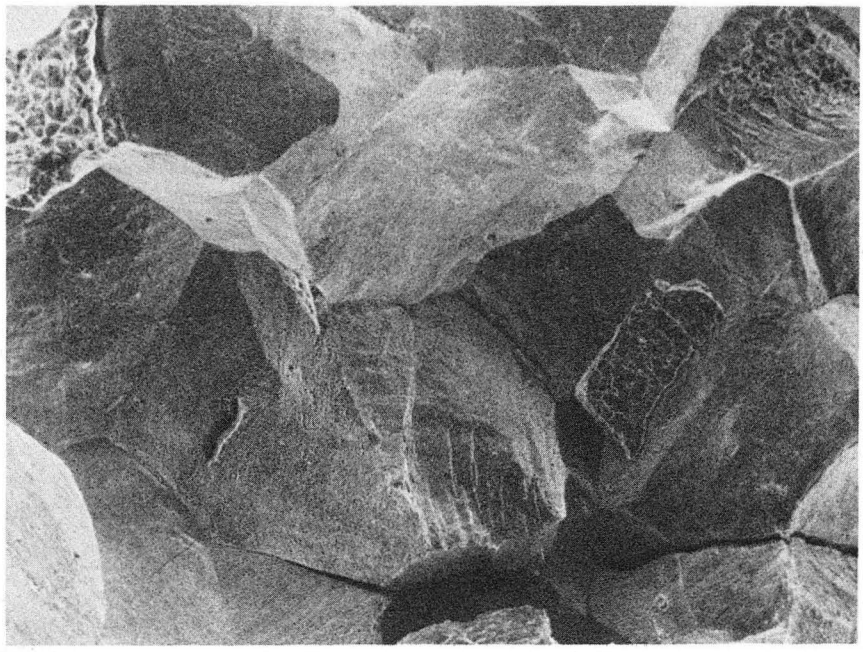

a

b

XBB760-10566

Fig. 12

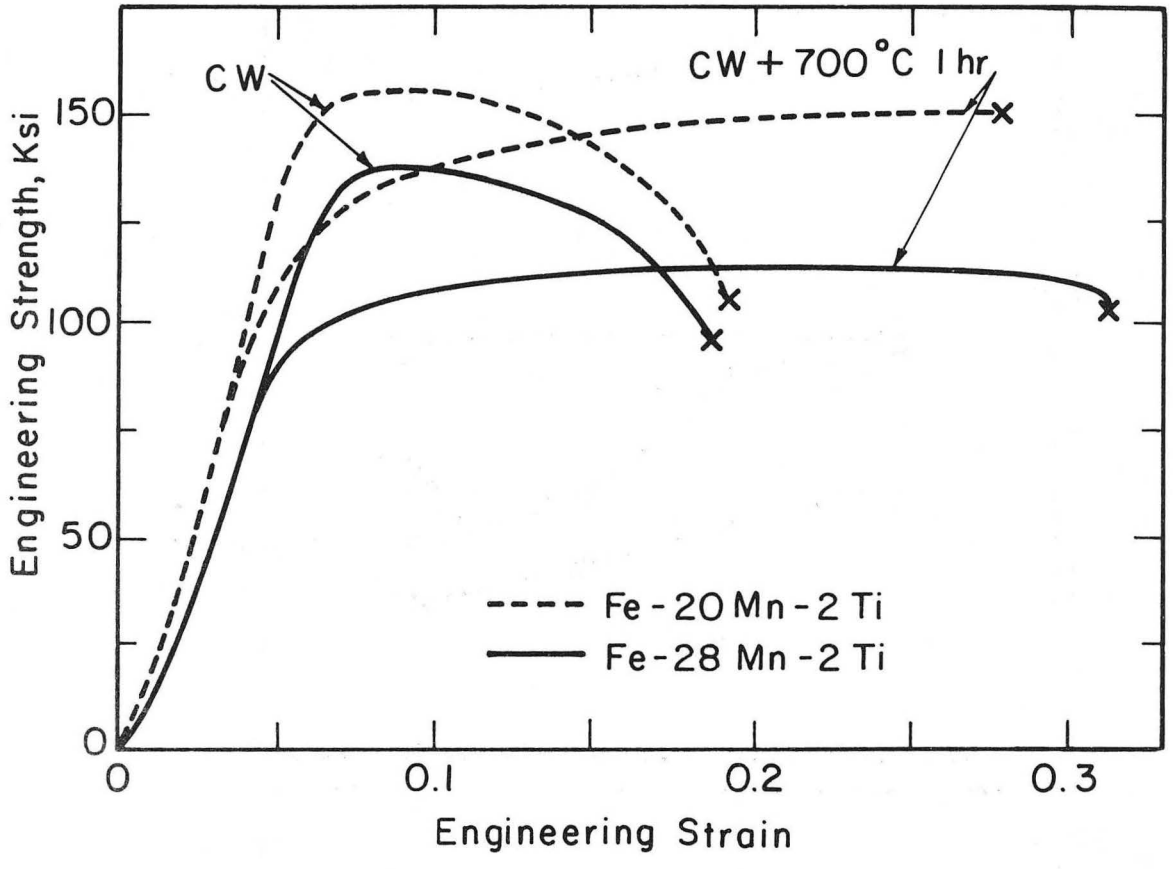

Fig. 13

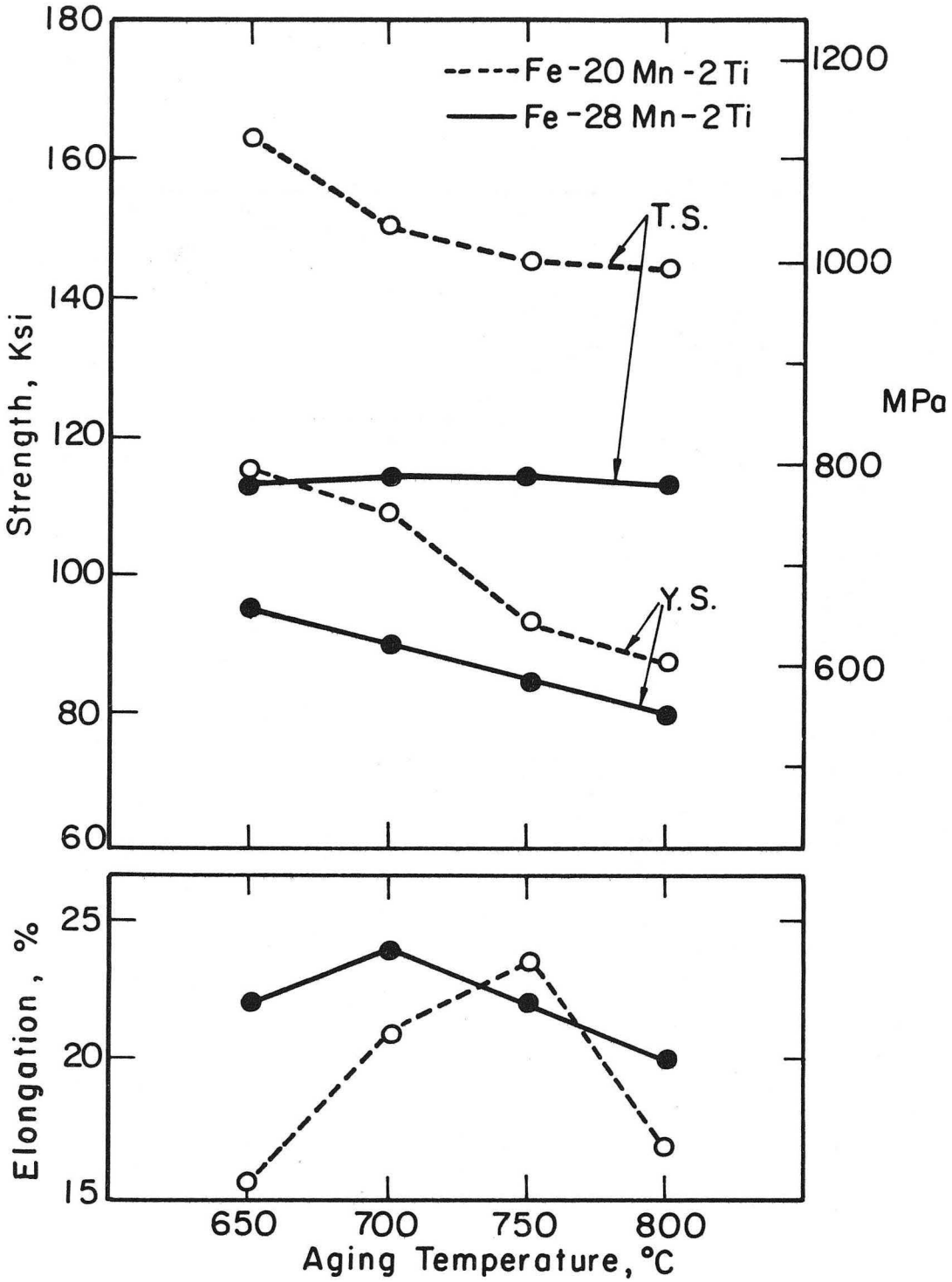
180
160
140
120
100
80
60
Strength, Ksi
1200
1000
800
600
MPa
Fe-20 Mn-2 Ti
Fe-28 Mn-2 Ti
T.S.
Y.S.
25
20
15
Elongation, %
650
700
750
800
Aging Temperature, °C
XBL778-5876

Fig. 14

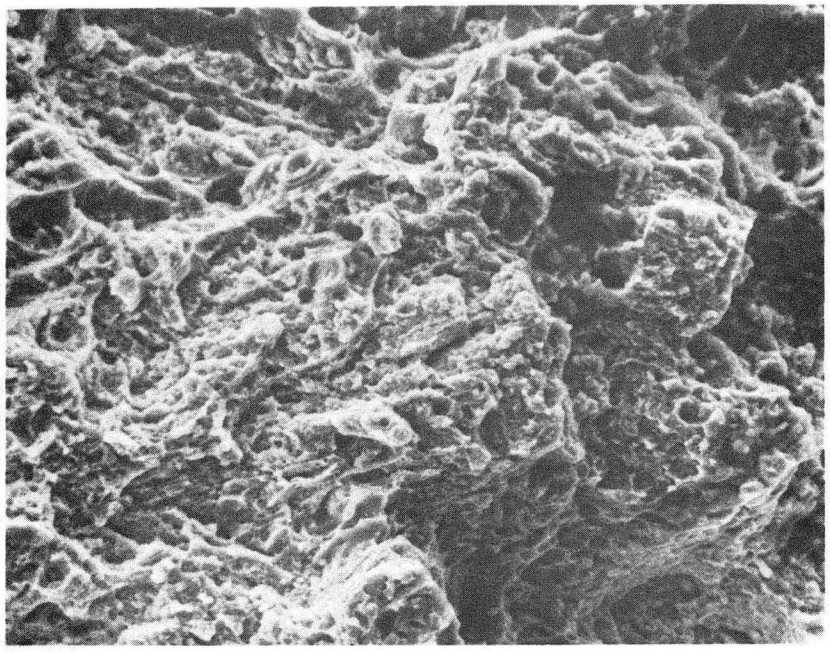

a

10 μm

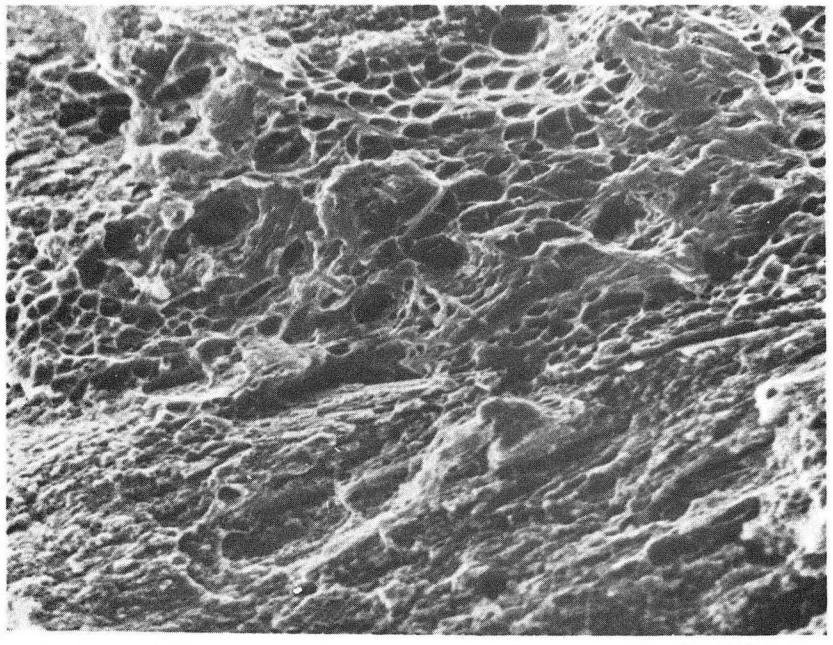

b

XBB778-7377

Fig. 15

TECHNICAL INFORMATION DEPARTMENT
LAWRENCE BERKELEY LABORATORY
UNIVERSITY OF CALIFORNIA
BERKELEY, CALIFORNIA 94720